CHAPTER V
THE EFFECT OF Ga AND Zn OVER HZSM–5 ON THE TRANSFORMATION OF PALM FATTY ACID DISTILLATE (PFAD) TO AROMATICS

(Published in Catalysis Communication)

5.1 Abstract

The catalytic conversion of PFAD (palm fatty acid distillate) to aromatics has been studied over HZSM-5, Ga/HZSM–5, and Zn/HZSM–5 catalysts. The presence of both Ga and Zn promoted the aromatization of PFAD. The higher aromatics yield of Zn/HZSM–5 was achieved by the presence of two zinc species; exchanged Zn^{2+} promoting the dehydrogenation of paraffins and ZnO promoting the decarboxylation of oxygenates. The shifting from decarbonylation over Brønsted acid site of the parent HZSM–5 to decarboxylation over ZnO preserved the Brønsted acid site for the aromatization, thus increasing aromatics yield.

Keywords: Reaction pathway, Zn/ZSM–5, Ga/ZSM–5, PFAD, Aromatics

5.2 Introduction

Aromatics, including benzene, toluene, ethylbenzene and xylene (BTEX), are widely used as feedstocks in petrochemical industry. Generally, the catalytic reforming of heavy naphtha and the aromatization of light paraffins are the main routes for producing aromatics [1]. However, as the depreciation of crude petroleum reserves and the rapid growth of aromatics demand, alternative routes from sustainable sources become attractive [2]. There are numerous alternative sources, reported as feedstocks to produce aromatics, including but not limited to methanol [3], ethanol derived from biomass [4], isobutyl alcohol [5], and glycerol [6]. Nevertheless, due to their high oxygen contents in the molecules, the feasibility to economically apply this process is still a matter of dispute.

Palm fatty acid distillate (PFAD) is a by–product from the steam distillation of crude palm oil [7]. To avoid the soap formation during the transesterification in biodiesel production, the deacidification is required to remove these free fatty acids first [8]. The conversion of PFAD to valuable products has gained increasing attention because not only allowed biodiesel competed economically with petroleum diesel but also provided the alternative low cost feedstock for producing renewable fuels. PFAD has been reported as a feedstock for producing biodiesel [9], hydrocarbons in diesel range [10], and hydrogen [11].

Herein, we reported the transformation of PFAD to aromatics. It should be noted that compared with other renewable feedstocks, PFAD has significant lower oxygen contents, non food competition, and sustainable amount in the future. In order to attain the selective formation of aromatics, HZSM–5 zeolite was selected as the catalyst. By the unique three–dimensional micropore system that consists of straight and zigzag channels coupled with a suitable shape selectivity and acid properties, HZSM–5 is accepted as the superior catalyst for aromatization of biomass–derived feedstocks [12-14].

It was proved that the incorporation of dehydrogenation metals on HZSM–5 catalysts significantly improved aromatics yield [15-19]. By the recent infrared study [20], gallium loaded on HZSM–5 catalyst was expected to be the active site for light paraffins activation due to the high activity in heterolytic dissociative adsorption and high activity in dehydrogenation of ethane. However, L. Yu and co–workers reported that by shifting the feedstock from light hydrocarbon to biomass derived alcohol, among the dehydrogenation metals (Zn, Ga, Mo, La, Ni. Ag, and Pt), Zn exhibited the highest activity in aromatization [5]. Therefore, in order to compare the catalytic activity in transformation of PFAD to aromatics, the same amount of both metals (Ga, and Zn) was impregnated on HZSM–5 catalysts. The effects of metal species on the catalytic activity were also investigated.

5.3 Experimental

5.3.1 Catalyst Preparation

The NH_4ZSM-5 zeolites with SiO_2/Al_2O_3 ratios of 23, 30, and 50 were obtained from Zeolyst International, USA. In order to convert to proton form, the catalysts were calcined in air at 550 °C for 5 h after that ground and sieved to the size between 20–40 mesh (450–850 μm). The $Zn(NO_3)_2$ or $Ga(NO_3)_3$ precursors were loaded on 3 g HZSM–5 (SiO_2/Al_2O_3 = 30) by incipient wetness impregnation (IWI) method. After that, the catalysts were dried at 110 °C overnight and then calcined in air at 550 °C for 5 h. The resulting catalysts are denoted as xM/HZSM–5, where x represents amount of expected metal loading and M represents Ga or Zn.

5.3.2 Catalytic Characterization

The prepared catalysts were characterized by various techniques. The atomic absorption spectroscopy (Varian SpectrAA 300) was used to determine the Zn and Ga contents in the prepared catalysts. Surface area and micropore volume of the prepared catalysts were measured by Brunauer Emmet–Teller (BET) method on a Quantachrom/Autosorb 1–MP instrument. The temperature programmed desorption of isopropylamine (IPA–TPD) was performed in a homemade apparatus using a quarter inch quartz tube reactor connected to an online MS detector (MKS Cirrus series 903). The catalysts were pretreated by heating under the He flow at 500 °C for 1 h and cooling down to room temperature. IPA was pulsed under the He flow until saturation was reached. The IPA–TPD was carried out in the range of 30–800 °C with a heating rate of 10 °C/min. The relative crystallinities of the HZSM–5 zeolites before and after loading metal were analyzed by a Rigaku X–ray diffractometer (XRD) with Cu tube for generating CuKα radiation (λ= 1.5418 Å) at room temperature. UV–vis spectra were recorded by UV–2550 under air atmosphere. The data was recorded in the range of 300–600 nm by using HZSM–5 (30) as a blank. The X–ray photoelectron spectroscopy (XPS) was conducted using a Kratos Ultra X–ray photoelectron spectrometer. The monochromatic AlKα was used as an X–ray source (anode HT = 15 kV). The binding energy of C (1s) at 285 eV was used as a reference.

5.3.3 Catalytic Activity Testing

Palm fatty acid distillate (PFAD) was obtained from Thai Oleochemicals Company Limited (TOL), Thailand. The reaction activity was tested in a continuous flow fixed bed reactor. The reaction was carried out at 500 °C under

atmospheric pressure. N_2 was used as a carrier gas with the flow rate of 55 mL/min. The PFAD was melted by preheating at 80 °C before feeding to the reactor. The gas products were analyzed on–line by using an Agilent Model 5890 gas chromatography equipped with a capillary HP–PLOT/Al_2O_3 "S" deactivated column for FID and Porapak N, 80–100 column for TCD detectors. The liquid products were analyzed by using an Agilent Model 6890 gas chromatography equipped with a capillary HP–INNOWAX column.

5.4 Results and discussion

5.4.1 Proposed Reaction Pathway for Converting PFAD to Aromatics

In order to study the reaction pathway, the product distribution of palm fatty acid distillated (PFAD) conversion to aromatics over HZSM–5 (SiO_2/Al_2O_3 = 30) catalyst as a function of space time (W/F) was investigated as shown in Fig. 5.1a.

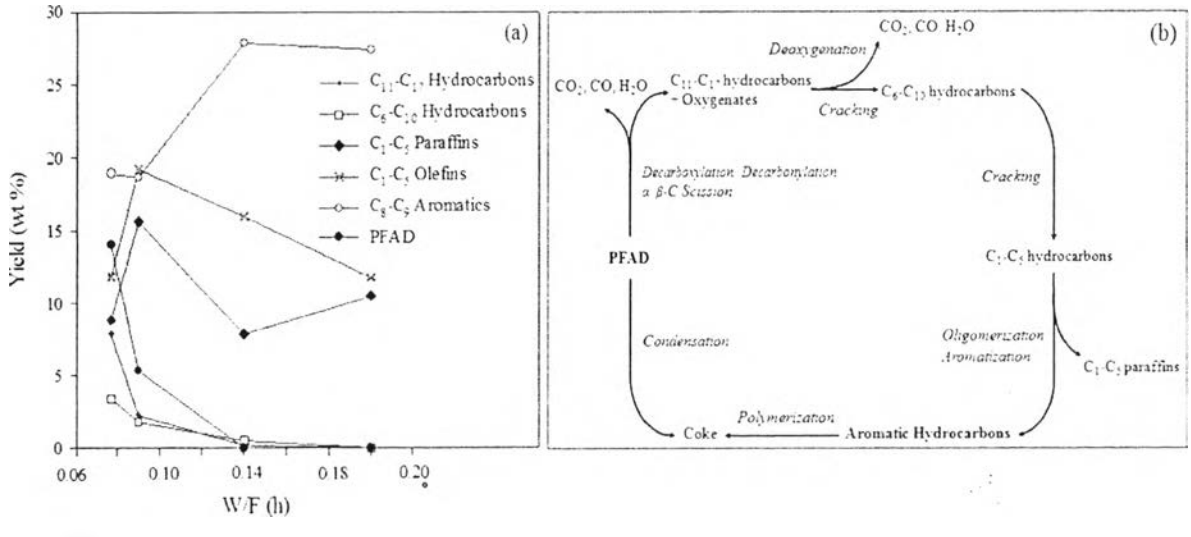

Figure 5.1 (a) Products yield of PFAD conversion over HZSM–5 as a function of space time (W/F). Reaction conditions: 500 °C, atmospheric pressure, and TOS = 3 h. (b) Proposed reaction pathway for the transformation of palm fatty acid distillate (PFAD) to aromatics.

Table 5.1 Fatty acid composition of palm fatty acid distillate (PFAD)

PFAD composition	wt %
Myristic ($C_{14:0}$)	1.2
Palmitic ($C_{16:0}$)	55.1
Stearic ($C_{18:0}$)	3.7
Oleic ($C_{18:1}$)	34.0
Linolenic ($C_{18:2}$)	6.1

From the feed analysis (Table 5.1), PFAD was mainly comprised of palmitic acid (55.1 wt %) and oleic acid (34.0 wt %). As the first step, the deoxygenation of fatty acid could proceed via decarboxylation, decarbonylation, or directly cracking of fatty acid molecules, resulting in long chain hydrocarbons (C_{11}–C_{17}) [21, 22]. While, the deoxygenation of resulted oxygenates produced CO, water, and CO_2 following the decarbonylation and decarboxylation reactions [23]. The C_{11}–C_{17} hydrocarbons were further cracked at the external acid sites of HZSM–5, generating aliphatic hydrocarbons in the range of C_6–C_{10}. The C_6–C_{10} hydrocarbons were then cracked and diffused into the HZSM–5 pores [24]. As the space time increased to 0.09 h, the formation of C_1–C_5 paraffins and olefins were significantly improved. It was believed that the oligomerization of light olefins produced a mixture of heavier olefins and paraffins, passing through alkylation, isomerization, and aromatization to produce aromatics [25]. As confirmed by the product distribution at W/F = 0.14 h, the raising in aromatics yield was achieved by declining of light olefins. As a consequence, coke was also generated by polymerization of the resulting aromatics or direct condensation of PFAD. The reaction pathway for transformation of PFAD to aromatics is proposed in Fig. 5.1b.

5.4.2 Transformation of PFAD over HZSM–5, Ga/HZSM–5, and Zn/HZSM–5 Catalysts

The effects of SiO_2/Al_2O_3 ratios in HZSM–5 on the conversion of PFAD to aromatics were studied by varying the SiO_2/Al_2O_3 ratios (23, 30, and 50).

The surface area and the Brønsted acidity of the catalysts are shown in Table 5.2. Compared to the others, HZSM–5 (30) provided the highest surface area whereas HZSM–5 (23) showed the highest Brønsted acidity. It was accepted that the increase in SiO_2/Al_2O_3 ratios results in lower the Brønsted acid site of the zeolite, leading to the lower catalytic active site for these reactions.

Table 5.2 Analysis of Zn loading, textural properties, and acidity of parent HZSM–5, Ga/HZSM–5, and Zn/HZSM–5 catalysts

Catalyst	SiO_2/Al_2O_3	Metal loading [a] (wt %)	S_{BET} (m^2/g_{cat})	Brønsted acidity [b] ($\mu mol/g_{cat}$)
HZSM–5	23	–	334.2	435
HZSM–5	30	–	375.7	377
HZSM–5	50	–	356.3	261
3Ga/HZSM–5	30	2.75	333.8	307
1Zn/HZSM–5	30	0.91	334.0	234
3Zn/HZSM–5	30	2.92	309.6	141
5Zn/HZSM–5	30	4.83	295.6	104
7Zn/HZSM–5	30	6.38	283.5	82

[a] The actual metal loading of Ga and Zn were confirmed by AAS method.

[b] The acidity was determined from IPA–TPD. The mass monitored was propylene (*m/e = 41*).

However, we believed that during the reaction the strong Brønsted acid sites of HZSM–5 (23) led to formation of coke, blocking the pore of the catalyst and resulting in lower catalytic activity. As a result (Fig. 5.2a), HZSM–5 (30) which provided both the highest surface area and suitable Brønsted acid site showed the higher aromatics yield (36 wt %) than HZSM (23) (29 wt %).

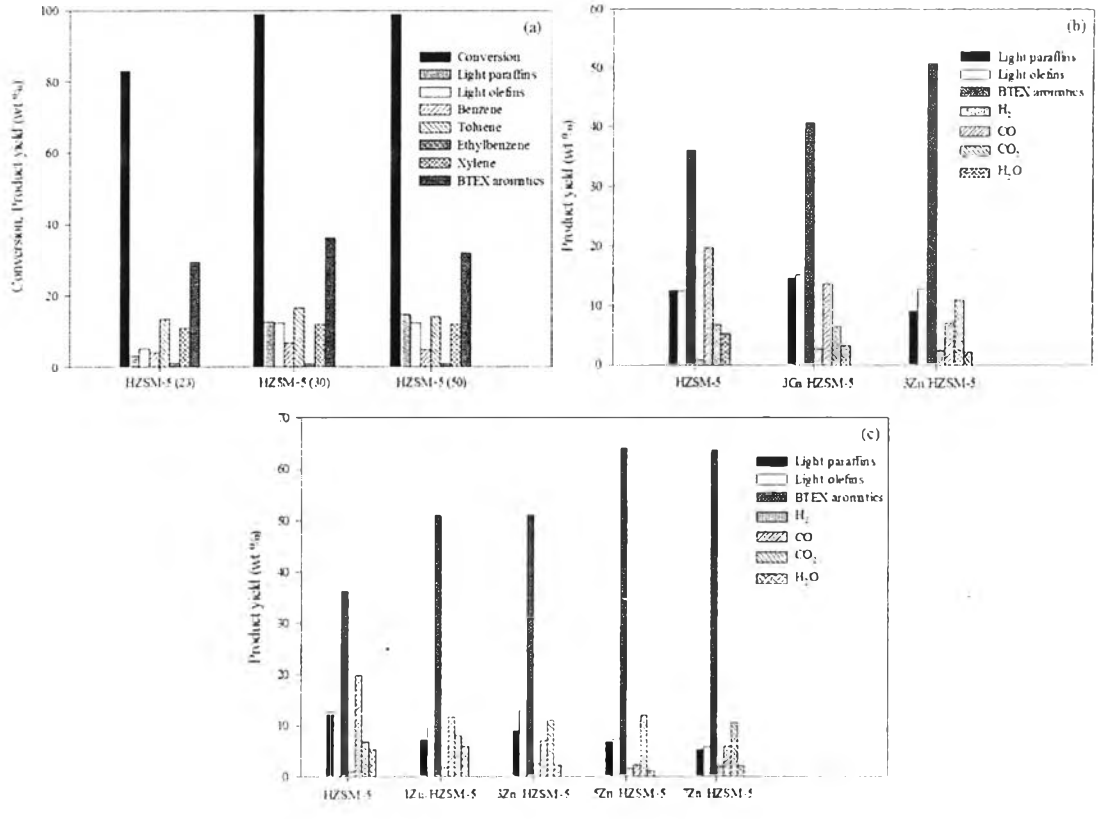

Figure 5.2 (a) PFAD conversion and products yield over parent HZSM–5 as a function of SiO_2/Al_2O_3 ratios, (b) Products yield of PFAD conversion over parent HZSM–5, 3Ga/HZSM–5 and 3Zn/HZSM–5 catalysts, and (c) Products yield of PFAD conversion over parent HZSM–5, 1Zn/HZSM–5, 3Zn/HZSM–5, 5Zn/HZSM–5 and 7Zn/HZSM–5 catalysts. Reaction conditions: atmospheric pressure, 500 °C, WHSV = 5 h^{-1}, TOS = 3 h.

In order to enhance the aromatics yield, two types of dehydrogenation metal, Ga and Zn, were impregnated on HZSM–5 (30) catalyst. As shown in Table 5.2, the presence of Ga and Zn decreased the surface area of the parent HZSM–5 catalyst from 375.7 to 333.8 and 309.6 m^2/g_{cat}. The Brønsted acidity was investigated by using temperature programmed desorption of isopropylamine (IPA–TPD). The decomposition of isopropylamine to propylene and ammonia over Brønsted acid site allows us to do the quantitative analysis of the Brønsted acidity via the Hofmann elimination reaction [26].

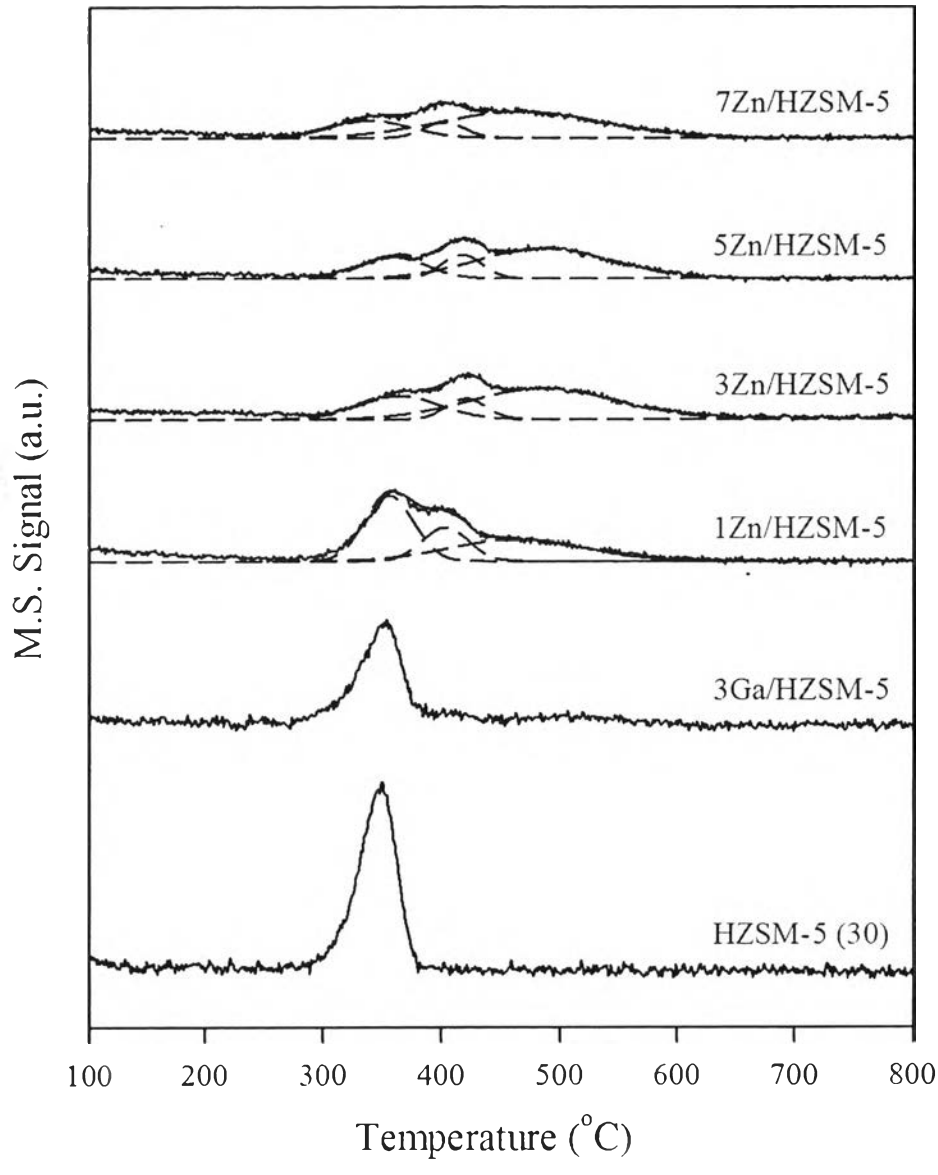

Figure 5.3 Isopropylamine–TPD (IPA–TPD) profiles of parent HZSM–5, 3Ga/HZSM–5, 1Zn/HZSM–5, 3Zn/HZSM–5, 5Zn/HZSM–5, and 7Zn/HZSM–5 catalysts. The mass monitored was propylene (*m/e* = 41).

Table 5.2 and Fig. 5.3 show the decrease of strong Brønsted acid site (350 °C) from 377 over parent HZSM–5 to 307 and 141 μmol/g_{cat} over 3Ga/HZSM–5 and 3Zn/HZSM–5 catalysts respectively. The new two peaks of Zn/HZSM–5 catalyst at higher temperature might be induced by the contaminated water in IPA. Agreed with the previous work by El–Malki and co–workers, the hydrolysis of Zn at exchange site resulted in the recovery of Brønsted acid sites [27]. However, under the reaction temperature, the dehydroxylation of dissociated water molecule suggested to eliminate these recovery Brønsted acid sites, led to the remaining of only acid site at 350 °C (141 μmol/g_{cat}). It was important to note that even at the same amount of metal loading, the significant difference of the remaining Brønsted acidity was observed. In the case of 3Ga/HZSM–5 catalyst, the impregnation of gallium nitrate precursor led to the formation of Ga_2O_3 cluster as a dominant species. Without the reduction process, this species tended to be stable and did not exchange with Brønsted acid site [28, 29]. On the other hand, over 3Zn/HZSM–5 catalyst more than half of Brønsted acid site was exchanged with Zn^{2+} cations and formed the Zn at exchange site species. This hypothesis was confirmed by XPS, shown in Fig. 5.4a. Agreed well with IPA–TPD results, the XPS spectrum of 3Ga/HZSM–5 showed only Ga_2O_3 species at 1118.3 eV [30]. The fitting of Zn $2p_{3/2}$ XPS spectrum showed two types of Zn species (Fig. 5.4b). The lower binding energy (1022.3 eV) was ZnO cluster whereas the higher binding energy (1023.3 eV) was dedicated to Zn at exchange site species. The shifting to higher binding energy was induced by the higher electronegativity of lattice oxygen in the zeolite framework [3].

All the three catalysts, HZSM–5, 3Ga/HZSM–5, and 3Zn/HZSM–5 were tested for their catalytic activity in the transformation of PFAD to aromatics, as shown in Fig. 5.2b. Even though, the incorporation of both Zn and Ga increased the aromatics yield, the significant increase was found over 3Zn/HZSM–5 catalyst. The introduction of Zn increased the aromatics yield to 51 wt % while 3Ga/HZSM–5 gave a lower yield at 41 wt %. It should be emphasized that not only aromatics yield but also CO and CO_2 formation were affected by Zn loading. Starting with the parent HZSM–5 catalyst, the Brønsted acid site rather enhanced the decarbonylation more than decarboxylation reactions, resulting in high amount of CO (20 wt %) and lower

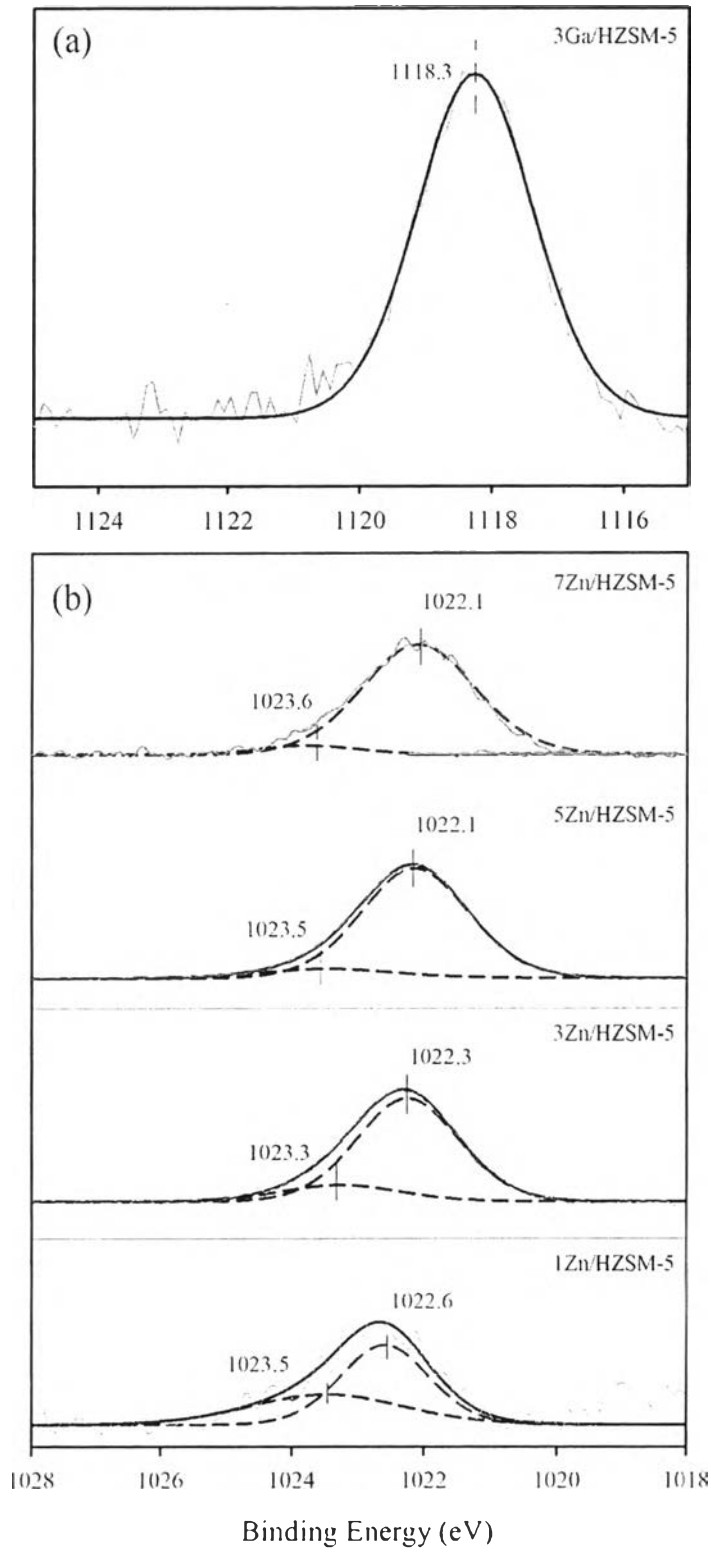

Figure 5.4 XPS spectra; (a) Ga ($2p_{3/2}$) of 3Ga/HZSM–5 and (b) Zn ($2p_{3/2}$) of 1Zn/HZSM–5, 3Zn/HZSM–5, 5Zn/HZSM–5, and 7Zn/HZSM–5 catalysts.

amount of CO_2 (7 wt %) [31]. Similar to the parent HZSM–5, 3Ga/HZSM–5 catalysts gave the dominant amount of CO (14 wt %) with a small amount of CO_2 (6 wt %). According to the IPA–TPD and XPS results, the stable form of Ga_2O_3 species led to the preserving the Brønsted acid site that could perform the decarbonylation reaction. On the contrary, the different phenomenon was found over 3Zn/HZSM–5 catalyst, the formation of CO was decreased to 7 wt % whereas CO_2 formation significantly increased to 11 wt %. It is possible that the introduction of zinc might shift the deoxygenation pathway from decarbonylation to decarboxylation reactions. In order to explain the roles of Zn to the aromatization and deoxygenation reactions, the products distribution as a function of Zn loading were investigated.

5.4.3 Transformation of PFAD to Aromatics over xZn/HZSM–5 Catalysts

The effects of Zn on the catalytic activity were studied by varying amount of Zn loadings (1, 3, 5, and 7 wt %). The actual metal loadings and textural properties are illustrated in Table 5.2. The XRD results show that the zeolite structures were preserved even at the highest amount of metal loading (not shown). As shown in Fig. 5.4b, XPS revealed two types of Zn species as previously mentioned. Moreover, it was important to note that by increasing Zn loading, the ZnO species (lower binding energy peak) became the dominant peak. Even though, XPS is one of the most powerful techniques to study the metal species; the provided information is only on the surface of the catalysts. In addition, IPA–TPD was also performed to do the bulk analysis of Zn/HZSM–5 catalysts (Fig. 5.3 and Table 5.2). In contrast with the strong Brønsted acidity (350 °C), the new peaks at higher temperature which are represented to the Zn at exchange sites increased with amount of Zn loading. The results implied that not only ZnO but also Zn at exchange site was increased.

The effects of Zn loading on the catalytic activity are shown in Fig. 5.2c. The continued increase in Zn loading significantly improved the aromatics yield with the decline of light paraffins. The highest aromatics yield was achieved over 5Zn/HZSM–5 catalyst with 64 wt % while light paraffins reached the minimum at 7 wt %. Agreed with previous works, the exchange of strong Brønsted acid site with Zn^{2+} cations led to the suppression of the cracking and hydrogen transfer reactions to the formation of light paraffins. In addition, the high activity in

dehydrogenation of the Zn at exchange site also improved the formation of olefins, precursor for producing aromatics [5]. On the contrary, it was noticed that the further increase in Zn loading to 7 wt % (7Zn/HZSM–5 catalyst) did not improved aromatics yield as expected. One might suggest that the increase in metal loading can lead to the block of the pore and lower the active site for aromatization. Notwithstanding, the BET surface area (Table 5.2) and XRD results confirmed the insignificant difference between 5Zn/HZSM–5 and 7Zn/HZSM–5 catalysts. These results implied that besides the Zn at exchange site there must be other factors effecting the conversion of PFAD to aromatics.

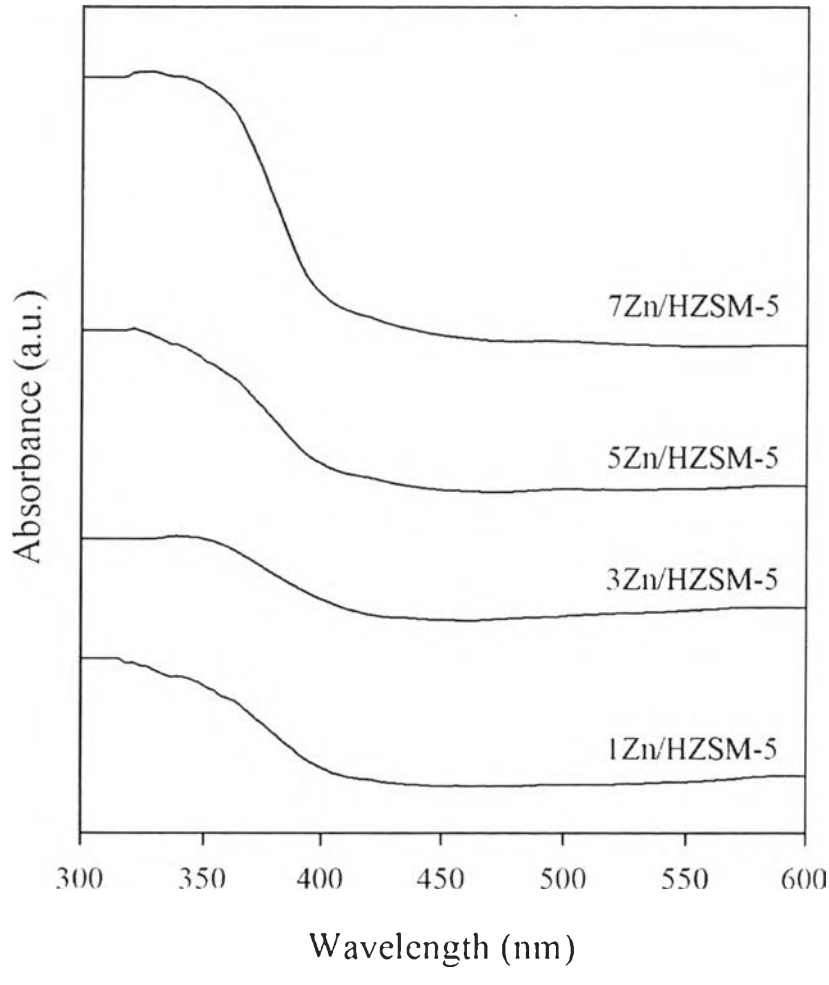

Figure 5.5 UV–vis absorption spectra of 1Zn/HZSM–5, 3Zn/HZSM–5, 5Zn/HZSM–5, and 7Zn/HZSM–5 catalysts.

Focusing on the by–products from deoxygenation reaction which are shown in Fig. 5.2c, the yield of CO obviously decreased while CO_2 increased with amount of Zn. It should be emphasized again that the increase in Zn loading not only led to the increase in Zn at exchange site but also ZnO species. Sugiyama *et al.* illustrated that ZnO performed the superior catalytic activity in decarboxylation of acetic acid, generated almost 100% CO_2 [32]. The shifting of deoxygenation pathway from decarbonylation on Brønsted acid site to decarboxylation on ZnO species might result in preserving the Brønsted acid site for the aromatization reaction.

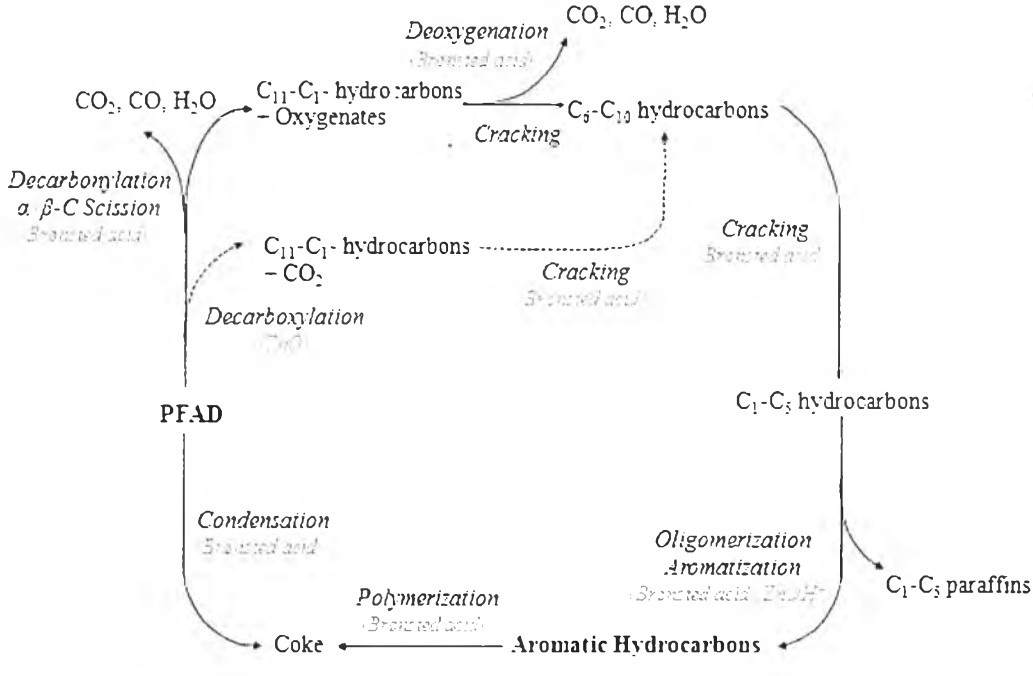

Figure 5.6 Proposed the effect of Zn species on Zn/HZSM–5 catalyst to the reaction pathway for the transformation of palm fatty acid distillate (PFAD) to aromatics.

As shown in Fig. 5.5, the band at 370 nm of UV–vis spectra corresponded to ZnO crystallites [33]. Although, the increase in Zn loading led to the development of this band, the intensive band was clearly observed on 7Zn/HZSM–5 catalyst indicating to the formation of large ZnO crystallites. It has been reported that the high amount of Zn impregnated on HZSM–5 catalyst led to the formation of large ZnO crystallites [34, 35]. This hypothesis was also confirmed by their product

distributions in Fig. 5.2c. The reason that the continued increase in Zn loading to 7 wt % decreased CO_2 yield was due to the lower available active ZnO site, decreasing the decarboxylation reactivity. These results plausibly explained that the significant increase in aromatics yield over Zn/HZSM–5 catalysts was a result from the combinative effects between the dehydrogenation of Zn at exchange site and decarboxylation of ZnO species. To conclude the effects of Zn species, the role of Zn species to the reaction pathway for the transformation of PFAD to aromatics is proposed in Fig.5.6.

5.5 Conclusions

Herein, we reported the single step transformation of palm fatty acid distillate (PFAD) to aromatics over modified HZSM–5 catalysts. The reaction pathway was proposed by starting with the deoxygenation of fatty acid, generating heavy hydrocarbons and oxygenates. Over Brønsted acidic HZSM–5, the further cracking of heavy hydrocarbons generated light paraffins and olefins, passing through oligomerization and aromatization to produce aromatics. Meanwhile, the oxygenated compounds were deoxygenated via decarboxylation/decarbonylation reaction, generated CO_2, CO, and H_2O. The introducing of both Ga and Zn improved aromatics yield due to their dehydrogenation activity. However, as compared with Zn/HZSM–5, Ga/HZSM–5, mainly comprised of Ga_2O_3 species, showed the lower aromatics yield. The remarkably high aromatization activity of Zn/HZSM–5 was resulted from the presence of two zinc species; exchanged Zn^{2+} promoting the dehydrogenation of paraffins and ZnO promoting the decarboxylation of oxygenates. The shifting from decarbonylation over Brønsted acid site of the parent HZSM–5 to decarboxylation over ZnO preserved the Brønsted acid site for the aromatization, thus increasing aromatics yield.

5.6 Acknowledgements

The authors would like to acknowledge the financial support from Center of Excellence on Petrochemical and Materials Technology and the Petroleum and Petrochemical College, Chulalongkorn University, Thailand.

5.7 References

1. D.L. Ransley, Kirk–Orthmer Encyclopedia of Chemical Technology, 3rd ed., Vol. 4, in: M. Grayson, D. Eckroth (Eds.), Wiley-Interscience, New York, 1978, pp. 264.
2. G.W. Huber, A. Corma, Angew. Chem. Int. Ed. 46 (2007) 7184-7201.
3. X. Niu, J. Gao, Q. Miao, M. Dong, G. Wang, W. Fan, Z. Qin, J. Wang, Microporous Mesoporous Mater. 197 (2014) 252-261.
4. K.V.D. Borght, V.V. Galvita, G.B. Marin, Appl. Catal. A: Gen. 492 (2015) 117-126.
5. L. Yu. S. Huang, S. Zhang, Z. Liu, W. Xin, S. Xie, L. Xu, ACS Catal. 2 (2012) 1203-1210.
6. S. Tamiyakul, W. Ubolcharoen, D.N. Tungasmita, S. Jongpatiwut, Catal. Today 256 (2015) 325-335.
7. A.G.M. Top, Lipid Technol. 22 (2010) 11-13.
8. S. Zallaikah, C.C. Lai, S.R. Vali, Y.H. Ju, Bioresour Technol 96 (2005) 1889-1896.
9. H.J. Cho, S.H. Kim, S.W. Hong, Y.K. Yeo, Fuel Process. Technol. 104 (2012) 271-280.
10. Y.S. Ooi, R. Zakaria, A.R. Mohamed, S. Bhatia, Kinet. Model. Energy Fuels 18 (2004) 1555-1561.
11. N. Laosiripojana, W. Kiatkittipong, S. Charojrochkul, S. Assabumrungrat, Appl. Catal. A: Gen. 383 (2010) 50-57.
12. Y. Yu, X. Li, L. Su, Y. Zhang, Y. Wang, H. Zhang, Appl. Catal. A: Gen. 447-448 (2012) 115-123.

13. J. Jae, G.A. Tompsett, A.J. Foster, K.D. Hammond, S.M. Auerbach, R.F. Lobo, G.W. Huber, J. Catal 279 (2011) 257-268.
14. A.J. Foster, J. Jae, Y.T. Cheng, G.W. Huber, R.F. Lobo, Appl. Catal. A: Gen. 423-424 (2012) 154-161.
15. S.M.T. Almutairi, B. Mezari, P.C.M.M. Magausin, E.A. Pidko, ACS Catal. 2 (2012) 71-83.
16. F. Solymosi, J. Cserenyi, A. Szoke, T. Bansagi, A. Oszko, J. Catal. 165 (1997) 150-161.
17. Y.W. Zhang, Y.M. Zhou, H. Liu, Y. Wang, Y. Xu, P.C. Wu, Appl. Catal. A: Gen. 333 (2007) 202-210.
18. G. Giannetto, R. Monque, R. Galiasso, Catal. Rev.- Sci. Eng. 36 (1994) 271-304.
19. C.L. Yin, Y.R. Zhao, C.G. Liu, Fuel 84 (2005) 701-706.
20. V.B. Kazansky, I.R. Subbotina, A.A. Pronin, R. Schlogl, F.C. Jentoft, J. Phys. Chem. B. 110 (2006) 7975-7978.
21. T.M. Sankaranarayanan, M. Banu, A. Pandurangan, S. Sivasanker, Bioresour. Technol. 102 (2011) 10717-10723.
22. Y. Yang, Q. Wang, X. Zhang, L. Wang, G. Li, Fuel Process. Technol. 116 (2013). 165-174.
23. C.D. Chang, A.J. Silvestri, J. Catal. 47 (1977) 249-259.
24. T.Y. Leng, A.R. Mohamed, S. Bhatia, Can. J. Chem. Eng. 77 (1999) 156-162.
25. M. Guisnet, D. Lukyanov, Stud. Surf. Sci. Catal. 90 (1994) 367-378.
26. T.J.G. Kofke, R.J. Gorte, G.T. Kokotailo, W.E. Farneth, J. Catal. 115 (1989) 265-272.
27. El-M. El-Malki, R.A. van Santen, W.M.H. Sachtler, J. Phys. Chem. B. 103 (1999) 4611.
28. V.I. Yakerson, T.V. Vasina, L.I. Lafer, V.P. Sytnyk, G.L. Dykh, A.V. Mokhov, O.V. Bragin, Kh.M. Minachev, Catal. Lett. 3 (1989) 339-345.
29. J.F. Joly, H. Ajot, E. Merlen, F. Raatz, F. Alario, Appl. Catal. A: Gen. 79 (1991) 249-263.
30. I. Nowak, J. Quartararo, E.G. Derouane, J.C. Vedrine, Appl. Catal. A: Gen. 251 (2003) 107-120.

31. A. Ausavasukhi, T. Sooknoi, D.E. Resasco, J. Catal. 268 (2009) 68-78.
32. S. Sugiyama, K. Sato, S. Yamasaki, K. Kawashiro, H. Hayashi, Catal. Lett. 14 (1992) 127-133.
33. Y.G. Kolyagin, V.V. Ordomsky, Y.Z. Khimyak, A.I. Rebrov, F. Fajula, I.I. Ivanova, J. Catal. 238 (2006) 122-133.
34. J.A. Biscardi, G.D. Meitzner, E. Iglesia, J. Catal. 179 (1998) 192-202.
35. S.M.T. Almutairi, B. Mezari, P. Magunsin, E.A. Pidko, E.J.M. Hensen, ACS Catal. 2 (2012) 71-83.